Journal of Power Sources 212 (2012) 212–219

Contents lists available at SciVerse ScienceDirect

Journal of Power Sources

journal homepage: www.elsevier.com/locate/jpowsour

A Raman spectroelectrochemical study of potential-controlled benzenethiol desorption from Pt–Fe group alloy films

Michael B. Pomfret*, Jeremy J. Pietron

Chemistry Division, United States Naval Research Laboratory, 4555 Overlook Avenue SW, Washington, DC 20375, USA

ARTICLE INFO

Article history:
Received 15 February 2012
Received in revised form
4 April 2012
Accepted 5 April 2012
Available online 16 April 2012

Keywords:
Raman spectroscopy
Cyclic voltammetry
Platinum
Platinum alloys
Benzenethiol
PEM fuel cell

ABSTRACT

A combination of *in situ* Raman spectroelectrochemistry and cyclic voltammetric (CV) stripping methods is used to study the adsorption/desorption of benzenethiol (BT) at platinum (Pt) alloy electrodes. The data from both methods confirm that alloying Pt with Fe group metals enhances the sulfur tolerance of the alloy over Pt. The Raman signal of BT adsorbed at electrodeposited films of Pt_3Co and Pt_4Ni diminishes to a greater extent after only one oxidation/reduction cycle than that observed for BT adsorbed at pure Pt films. Oxidatively desorbed BT readsorbs at Pt_3Co at a potential that is ~50 mV lower than that at which it readsorbs at either Pt or Pt_4Ni films, further demonstrating its enhanced sulfur tolerance. Sulfate bands are absent from the spectra of all films, indicating that the metal–S bonds that form upon adsorption are broken during oxidative removal of BT rather than cleavage of C–S bonds in the BT adsorbate. The CV stripping data confirm that BT is more readily electrochemically stripped from the alloy films than from pure Pt films. The combination of Raman spectroelectrochemistry and CV stripping enables more comprehensive characterization of sulfur-tolerant electrocatalyst surfaces *in situ*, under electrochemical conditions.

Published by Elsevier B.V.

1. Introduction

Platinum (Pt) is the preferred catalyst for a variety of energy-related processes, including oxygen-reduction (ORR) and hydrogen oxidation (HOR) reactions in low-temperature fuel cells, C–H bond activation catalysis, and catalytic conversion of exhaust in automobiles [1–4]. While proton-exchange membrane fuel cells (PEMFCs) typically employ Pt as both anode and cathode catalyst, an ongoing challenge to PEMFC development is the high susceptibility of Pt to contamination from carbon- and sulfur-containing species. PEMFCs must be fuel-flexible to be widely adopted in industrial, military, and transportation sectors. Specifically, PEMFCs must tolerate operating with hydrogen derived from fuels currently available through existing infrastructure. Hydrogen fuel stocks generated by reforming hydrocarbon fuels typically contains significant amounts of contaminants such as carbon monoxide (CO), hydrogen sulfide (H_2S) and organosulfur compounds. Exposure to as little as 50 ppm of such species quickly degrades PEMFC performance [5].

The alloying of Pt with other metals, particularly the alloying of Pt with iron-group metals, has been heavily investigated as a means to both promote catalytic reactions and to alleviate poisoning of Pt. Stamenkovic et al. demonstrated that Pt alloyed with 3d transition metals, especially cobalt (Co) and nickel (Ni), binds oxygen ~0.2 eV more weakly than unalloyed Pt, leading to higher electrocatalytic ORR activity on both alloyed films and alloy nanoparticles [6]. Alloying Pt with Fe group metals to study the effect of tailoring the catalyst electronic state has been applied to a variety of catalytic reactions [7,8]. For example, Moffat et al. found that PtCo and PtNi films that are 25–35% Co or Ni have ORR activities that are more than twice that of Pt alone [9]. Furthermore, the Pt surface layer that results from dealloying the film is at least three times more active for ORR (per gram of Pt) than unalloyed Pt [9].

PtCo and PtNi nanoparticles have also been studied for tolerance to common fuel poisons. Pt–Fe group alloys are resistant to CO poisoning [10–12], making them attractive for use as HOR catalysts. The adsorption, desorption and catalysis poisoning effects of sulfur (S) species on Pt_3Co alloy particles have been investigated using electroanalytical methods, specifically rotating ring-disk electrode (RRDE) experiments, combined with DFT calculations [13]. While S species adsorb as readily to Pt_3Co alloy nanoparticles as to pure Pt nanoparticles, electrochemically clean surfaces on Pt alloys are more easily regenerated by potential cycling than on the pure Pt nanoparticles. This enhanced oxidative removal of S species from Pt_3Co alloy nanoparticles derives from

* Corresponding author. Tel.: +1 202 404 2554; fax: +1 202 404 8119.
E-mail address: michael.pomfret@nrl.navy.mil (M.B. Pomfret).

0378-7753/$ – see front matter Published by Elsevier B.V.
doi:10.1016/j.jpowsour.2012.04.010

the increased oxygen mobility in the Co-depleted outer Pt shell of the Pt_3Co catalyst [13].

To better understand the oxidative removal of S species from Pt and Pt alloys, and thus the sulfur-resistant nature of Pt alloys, we employ *in situ* Raman spectroelectrochemistry in combination with cyclic voltammetric (CV) methods. The identification of molecular species on electrocatalyst surfaces is critical to optimizing existing electrocatalysts and to developing new ones. *In situ* optical methods reveal which adsorbates bind to and desorb from the catalyst, as well as the identity of intermediate species, providing information that complements electrochemical data and serves to verify or correct proposed mechanistic models of catalysis and poisoning. Raman spectroscopy is a leading optical technique for *in situ* investigation of catalysts in electrochemical and fuel cell systems [14,15], and has been used to determine adsorbate–substrate interactions at PEMFC-relevant catalysts [16–20]. *In situ* spectroelectrochemical Raman studies of benzenethiol (BT) on Pt and Pd nanoparticle films showed that different mechanisms account for the removal of BT at oxidizing potentials on these two metals and that the interaction of S with PtPd alloy films is stronger than with Pt alone [19].

In the present study, films of alloyed PtCo, PtNi, and pure Pt are electrochemically deposited at gold electrodes with Pt:X atomic percentage ratios of ~3:1 for PtCo and ~4:1 for PtNi. Continuous metal films are produced in order to ensure strong adsorbate Raman signals and to eliminate interference from carbonaceous species associated with Vulcan carbon-supported Pt alloy electrocatalysts (typically 30 wt% Pt alloy nanoparticles on Vulcan carbon) [21,22]. Benzenethiol is adsorbed at the films as a model Raman-active sulfur probe. Electrochemically induced desorption and readsorption of chemisorbed BT are evaluated with Raman spectroscopy, revealing that both Pt_3Co and Pt_4Ni are resistant to readsorption of oxidatively stripped BT.

2. Experimental

2.1. Materials

Chloroplatinic acid hexahydrate ($H_2PtCl_6 \cdot 6H_2O$, Sigma–Aldrich, >37.5 wt% Pt basis), cobalt chloride ($CoCl_2$, anhydrous, 99.7%, Alfa Aesar), nickel chloride ($NiCl_2$, anhydrous, 99%, Alfa Aesar), benzenethiol (≥98%, Sigma–Aldrich), perchloric acid ($HClO_4$, GFS Chemicals, double-distilled), 2-propanol (Fisher, ACS plus grade) and ethanol (Warner-Graham Co., 200 proof absolute) were all used as-received. Silicon wafers (WRS) were trimmed to appropriate sizes (~1.5 cm × 5 cm), cleaned by sonication in 2-propanol and in an oxygen plasma (Plasma Preen) immediately before Ti and Au deposition. Marine epoxy (Loctite) was used as-received.

2.2. Preparation of metal films

The trimmed silicon wafers were coated with 25 nm of titanium and 100 nm of gold by e-beam deposition using a Temescal E-Beam Evaporator. Continuous Pt films were electrochemically deposited at the Au face of the Au/Ti/Si substrate, which served as the working electrode in a 3-electrode cell configuration (Pt gauze counter electrode and fritted Ag/AgCl 3 M KCl reference electrode from Bioanalytical Systems) from a deposition solution comprising 3 mM H_2PtCl_6/0.5 M Na_2SO_4. The applied potential (controlled by Gamry Reference 3000 Potentiostat/Galvanostat/ZRA) was cycled 25× at 100 mV s^{-1} between −0.1 V and 1.2 V versus standard hydrogen (SHE) potential (corrected from the Ag/AgCl potential). This method differed from that used to deposit the alloy films, as the potential step method used to co-deposit Pt and Co or Pt and Ni to yield the Pt_3Co and Pt_4Ni films (*vide infra*) was ineffective for depositing Pt alone. Pt alloy films were deposited as described by Moffat et al. [9]. An Au//Ti//Si electrode immersed at the non-depositing potential of +1.00 V versus SHE into the deposition bath containing 2 mM H_2PtCl_6 and either 0.1 M $CoCl_2$ or 0.1 M $NiCl_2$, with 0.5 M NaCl as the supporting electrolyte. A potential of −0.21 V was then applied for 10 min to deposit the alloy films. Sample composition is verified using X-ray photoelectron spectroscopy (XPS) (Thermo Scientific K-Alpha spectrometer) and X-ray diffraction (XRD) (Bruker AXS D8 Advance). The XPS measurements were made with monochromatic Al-Kα incident radiation (1486.6 eV), using a step size of 0.15 eV, a dwell time of 0.1 s. Each individual spectrum was recorded in fixed analyzer transmission (FAT) mode with a pass energy of 20 eV and an accumulation of 10 scans. All spectra were processed and fitted with Unifit 2007 software, using the minimum number of peaks consistent with the best fit. The 284.8 eV peak of adventitious carbon is used as a convenient reference, though no charging effects are observed on the metal films. The XRD measurements were made using 40 kV, 40 mA, Cu-Kα radiation. The data were collected in the 30–90°2θ range with a step range of 0.03° at 5 s per step.

2.3. BT adsorption to Pt and Pt alloy films

The Pt and Pt alloy film electrodes were sealed into spectroelectrochemical cells comprising plastic vials with marine epoxy as sealant, as described previously [19]. The potted electrodes were electrochemically cleaned by cycling between 50 mV and 1250 mV at 200 mV s^{-1} for 10 cycles in 0.1 M $HClO_4$. The films were then rinsed in Nanopure H_2O, followed by ethanol, and then immediately soaked in a ~0.01 M solution of BT in ethanol for 1 h. After the BT soak, excess BT was rinsed away with clean ethanol, after which the cell was filled with 0.1 M $HClO_4$(aq) electrolyte. Raman spectroelectrochemical or CV stripping measurements were subsequently performed.

2.4. Raman spectroelectrochemistry

The assembled spectroelectrochemical cell (Fig. 1), comprising 0.1 M $HClO_4$ as electrolyte, a platinum wire counter electrode, and an Ag/AgCl reference electrode (World Precision Instruments, Inc., FLEXREF), was placed under the objective lens (20×) of a Raman microscope (Renishaw Ramascope). The 514-nm line of an argon-ion laser was focused on the sample, and Raman scattered light was collected at 180° to the incident beam. Spectra were obtained with a resolution of 4 cm^{-1} and comprise 25 co-added scans, each with a duration of 10 s, taken at a constant potential. The spectra of BT adsorbed at Pt and Pt alloy films were acquired at various potentials from 200 mV to 1300 mV, and taken first in ascending potential increments, then in descending increments to track changes in the metal films and in the chemisorbed BT as a function of potential. In some cases a second ascending potential series of spectra were acquired.

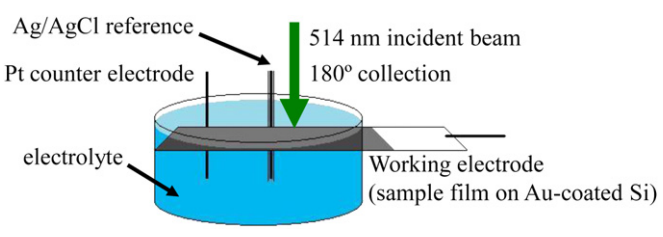

Fig. 1. Scheme of the spectroelectrochemical Raman cell used for *in situ* measurements on Pt and Pt alloy films.

2.5. CV stripping of BT from Pt and Pt alloy films

Electrochemical stripping of BT from the metal films was achieved by cycling between 100 mV and 1350 mV at 50 mV s^{-1} in 0.1 M $HClO_4$ until voltammetric waves either recover their appearance prior to BT exposure or reach a steady-state condition. All CV stripping measurements were controlled with a Pine Instruments AFCBP1 potentiostat controlled by a PC and Pinechem™ electrochemical software.

3. Results and discussion

3.1. X-ray characterization of Pt and Pt alloy films

The atomic composition and chemical state of the electrodeposited PtCo and PtNi alloy films were examined with XPS to confirm that the multicomponent films exhibited the expected Pt:X ratios (Fig. 2). Analysis of data from several locations on the alloy films gives an average Pt/Co ratio of ~2.7 ± 0.5 and an average Pt/Ni ratio of ~3.8 ± 1.4, close to the target ratios of 3:1 and 4:1, respectively. The fitted spectral component peak positions of the alloys (Table 1) agree with values reported elsewhere for these alloys [10,23–25]. No shift is seen in the Pt $4f_{7/2}$ peak of Pt_3Co from the standard value of 71.2 eV attributed to Pt metal [25], as has been reported elsewhere for Pt_3Co [24]. In Pt_4Ni, the Pt $4f_{7/2}$ peak shifts positively by 0.2 eV to 71.4 eV due to the presence of Ni reducing the final-state screening in Pt, causing the core binding energy to increase [26–28]. The presence of peaks corresponding to Ni and Co oxides in the Ni 2p and Co 2p spectra for the respective alloys shows that both Ni and Co atoms on the surface of the films are partially oxidized by ambient exposure after the films have been deposited, in agreement with results published by Shukla et al. that show some degree of oxidation at the surface of Pt_x(Co/Ni) alloy particles [24]. XPS is extremely sensitive to the surface environment, only probing the first few nanometers. The doping metals are not likely to be extensively oxidized throughout the depth of the films.

The X-ray diffraction (XRD) data (Fig. 3) confirm that the electrodeposited mixed metal films are predominantly alloys. The film thicknesses are ≤100 nm, allowing very strong reflections from underlying Au and Si layers to appear in the diffraction pattern. Neither Ni nor Co crystalline structure is seen in the Pt_3Co or Pt_4Ni films, in agreement with published results of alloys with similar, majority Pt compositions [9,29]. The Pt(111) peak, observed at 39.9° in the Pt film, diminishes to a weak peak at 42.0° in the Pt_3Co film and a shoulder at 40.8° in the Pt_4Ni film. The behavior of this peak is a result of the incorporation of Co and Ni atoms into the Pt face-centered cubic (fcc) crystal lattice, causing expansion and, in turn, broadening and weakening the Pt(111) reflection [9,29].

Table 1
XPS elemental analysis of Pt, Pt_3Co and Pt_4Ni films.

Film	Element	Atomic %	Components/eV	Assignment
Pt	Pt $4f_{7/2}$	100	71.2	Pt
			71.6	PtO
Pt_3Co	Pt $4f_{7/2}$	74.3	71.2	Pt
			71.9	PtO
	Co $2p_{3/2}$	25.7	780.6	Co^{2+}
			783.0	Satellite
			785.7	Satellite
			787.9	Satellite
Pt_4Ni	Pt $4f_{7/2}$	81.6	71.4	Pt
			71.8	PtO
	Ni $2p_{3/2}$	18.4	852.6	Ni
			855.7	Ni_2O_3
			858.0	NiO
			860.8	Satellite
			863.4	Satellite

3.2. Raman spectroelectrochemistry of BT adsorption/desorption at Pt and Pt alloy films

The potential-dependent electrochemical behavior of BT adsorbed at Pt films electrodeposited on Au//Ti//Si electrodes serves as a control to compare with the behavior of BT adsorbed at Pt_3Co and Pt_4Ni films electrodeposited on Au/Ti/Si. Potential-dependent Raman spectra were taken of BT adsorbed at a Pt film poised initially at 200 mV, then in ascending 150 mV increments to 1300 mV, followed by descending 150 mV increments back to

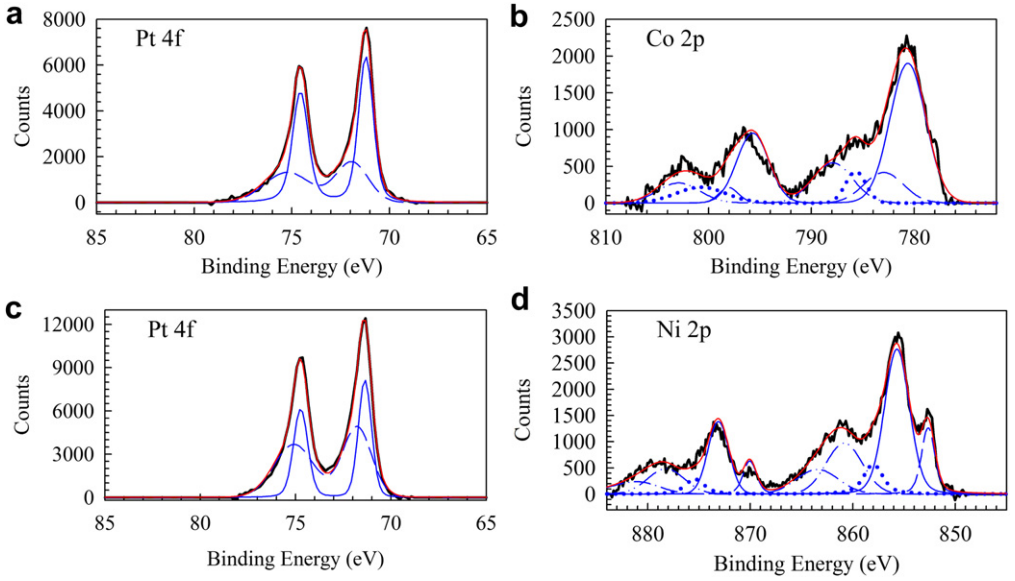

Fig. 2. The XPS data for the a) Pt 4f region and b) Co 2p region of a Pt_3Co alloy film; and the c) Pt 4f region and d) Ni 2p region of a Pt_4Ni alloy film. Parameters derived from fitting the bands are displayed in Table 1.

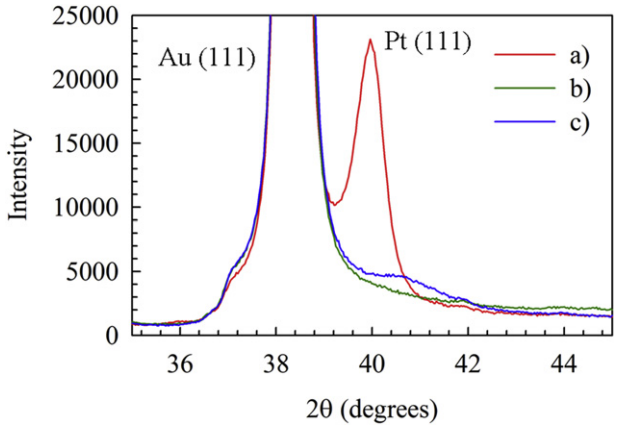

Fig. 3. XRD data for a) Pt, b) Pt_3Co, and c) Pt_4Ni films.

200 mV. When adsorbed at a metal surface, BT is oriented at 76° off of the surface normal and typically exhibits four sharp peaks assigned to the υ_{12}, υ_{18a}, υ_1, and υ_{8a} C–C modes—at 1000, 1021, 1064, and 1572 cm^{-1}, respectively [30,31].

The 1572 cm^{-1} peak is used to determine the extent of BT coverage on the Pt film, as it features the best signal-to-noise ratio of any of the peaks and provides the clearest indication of the potentials at which BT desorbs and readsorbs (Fig. 4a, only selected spectra shown for clarity). The intensity of this peak at all potentials relative to the intensity of the 1570 cm^{-1} peak measured at 200 mV is plotted versus potential in Fig. 4b. The relative scattering signal increases at intermediate potentials, which arises as the ring of the BT reorients more parallel to the electrode surface as induced by charge-transfer interactions at the lower applied potentials, resulting in decreased intensity of the angle-specific BT Raman bands [31,32]. After reaching a maximum relative intensity between 700 and 1000 mV, the signal starts to decline at more positive potentials, coinciding with onset of Pt oxidation. At 1300 mV, all BT modes are completely gone. The υ_{8a} mode at 1572 cm^{-1} reappears at 850 mV during the negative-going potential increments, returns to its initial intensity at 700 mV, and exceeds it at 200 mV. The increase in signal is attributed to electrochemical roughening of the Pt surface leading to modest surface enhancement in the Raman signal of BT on Pt [33]. This disappearance and subsequent reappearance of the BT Raman signature as a function of potential is consistent with our previous observations [19] that the Pt–S bond breaks upon formation of Pt oxide (Eq. (1)):

$$\mathrm{Ph{-}S{-}Pt + 3H_2O \rightarrow Pt + PhSO_3^- + 6H^+ + 5e^-} \quad [1]$$

where Ph represents the phenyl group in BT. A hydrophobic layer of benzenesulfonic acid remains nonspecifically adsorbed to the Pt electrode in acid electrolyte, with the Pt–S bond reforming at lower potentials as Pt oxide is reduced (the reverse of Eq. (1)) and benzenesulfonic acid is reduced back to the benzenethiolate. When BT is adsorbed at Pt_3Co (Fig. 5a) and Pt_4Ni (Fig. 5b) the same four Raman bands are evident. As with the Pt film, BT desorption from both alloy films begins at 1150 mV, as indicated by the reduction in BT Raman signal intensity, and culminates by 1300 mV, resulting in a total absence of the BT spectroscopic signature.

The Raman spectra of the Pt_4Ni surface collected during the negative-going potential increments behave similarly to those for the Pt film, with the BT Raman signature starting to return at 850 mV (Fig. 5b). However, BT readsorption at Pt_3Co occurs at more negative potentials than at Pt (Fig. 5a). The relative intensity plots

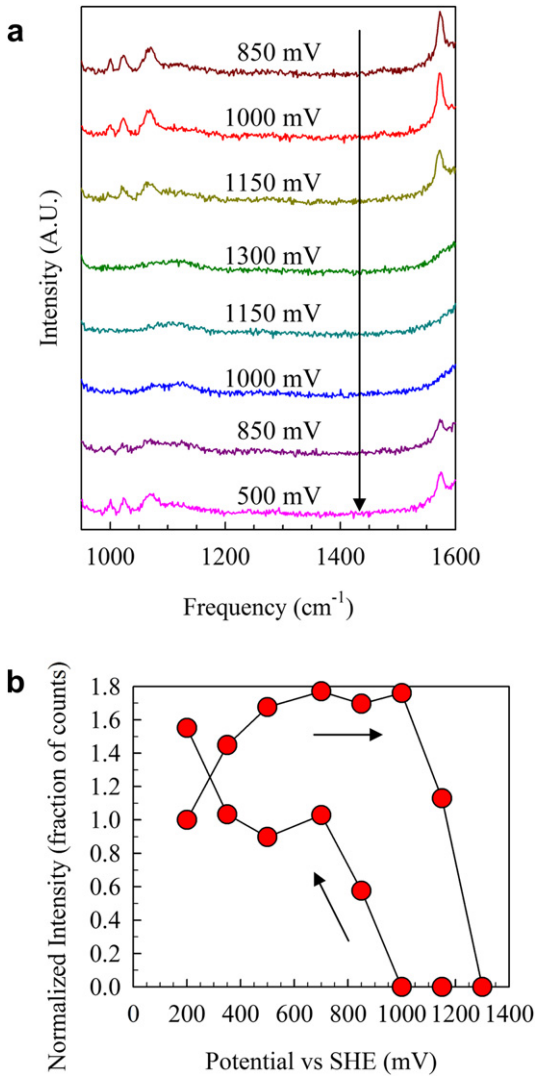

Fig. 4. a) *In situ* Raman spectra of a Pt film electrode exposed to a 0.01 M BT solution for 1 h. The potentials are shown versus SHE and proceed sequentially from top to bottom. b) Intensities—relative to the initial 200 mV measurement—of the 1570 cm^{-1} BT Raman peak for the same Pt film are plotted at all of the applied potentials for cycling to 1300 mV (→) and returning to 500 mV (←).

as a function of potential (Fig. 6) for the Pt_3Co and Pt_4Ni films show a clear difference between the pure Pt (Fig. 4b) and the alloy films over the course of the negative-going potential increments. The BT Raman signature reappears on Pt_3Co at 700 mV—a lower potential than for either Pt or Pt_4Ni—demonstrating that alloying Pt films with Co makes them more resistant to sulfur adsorption in electrochemical environments. At 200 mV, where the Pt_3Co film is oxide free, the BT Raman signal reaches only ~60% of the intensity observed after initial BT monolayer formation, prior to oxidizing the film. In the case of Pt_4Ni, the BT signal only reaches ~40% of the initial intensity. These diminished BT Raman signal intensities upon return to reducing potentials indicates that less BT readsorbs at the alloys than at pure Pt upon reduction of the metal film.

To determine the BT readsorption potential more precisely, a second set of spectroelectrochemical measurements was made using 50 mV increments in the desorption and readsorption regions of the electrochemical cycle, 1000–1300 mV and 1050–700 mV, respectively (Fig. 7). Desorption of BT from the Pt and Pt_3Co films during the positive-going increments matches the 150 mV step

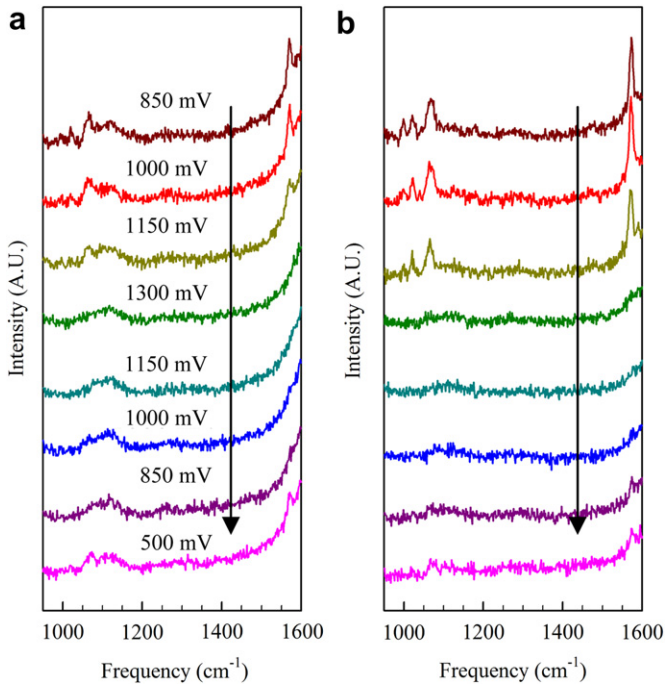

Fig. 5. a) *In situ* Raman spectra of a Pt_3Co film electrode and b) a Pt_4Ni film electrode to a 0.01 M BT solution for 1 h. The potentials are reported versus SHE and proceed sequentially from top to bottom.

data, with BT signal persisting until 1300 mV. The desorption potential for BT on Pt_4Ni film *decreases* to 1250 mV. This more facile desorption of BT from Pt_4Ni is corroborated by cyclic voltammetric stripping data (*vide infra*). Raman data from the negative-going increments confirm the enhanced resistance of Pt_3Co to BT readsorption.

It should be noted that readsorption of BT is observed at higher potentials on all films during the 50 mV step experiments than during the lower-resolution experiments, indicating that readsorption is a kinetically slow process. The time associated with the additional increments within the readsorption potential window allows the slow reduction of Pt oxides and concomitant readsorption of BT to proceed sufficiently to be detected at ~900 mV on Pt and Pt_4Ni. At this higher potential resolution, the BT Raman signal reappears on Pt_3Co films at 850 mV—higher than the value

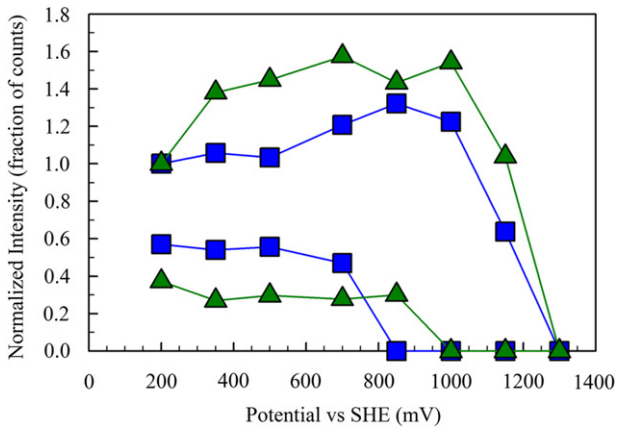

Fig. 6. Relative intensities of the 1570 cm^{-1} BT Raman peak at all potentials examined for (■) Pt_3Co and (▲) Pt_4Ni films exposed to 0.01 M BT solution for 1 h.

of 700 mV measured with the 150 mV increments—but still 50 mV lower than on the Pt and Pt_4Ni films.

Furthermore, at 200 mV, the BT signal on Pt_3Co is only ~25% as intense as when first deposited. This drop in intensity can also be attributed to the larger number of smaller potential steps between Raman scans, resulting in more time spent with the films poised at oxidizing potentials, during which oxidized BT can diffuse into solution. Similarly, restriction of the experiment to the desorption/adsorption potential window results in less time spent with the films poised at sufficiently reducing potentials for BT to readsorb. The Pt and Pt_4Ni films both recover 55–65% of their signal intensity; however, the relative BT signal is ~20% stronger on Pt than Pt_4Ni during a second positive-going potential sweep. During the second series of positive-going increments, BT fully desorbs from both the Pt_3Co and Pt_4Ni films at 1200 mV, 50 mV more negative than from the pure Pt films.

Previous work demonstrated that Raman spectroscopy can differentiate between desorption mechanisms involving the cleavage of the C–S bond in the BT molecule and those involving the breaking of the metal–sulfur bond [19]. In the case of C–S cleavage, S is left behind on the metal surface and is oxidized to sulfate species as more time is spent at high potentials, which appears as a broad feature in the Raman spectra between 1000 and 1200 cm^{-1} [19]. None of the three film compositions tested in the present study display this spectral feature, providing evidence that no residual adsorbed S species remains after BT desorbs. Features in the low-frequency region of the Raman spectra (Fig. 8) further confirm that the metal–S bond is broken during electrooxidative desorption of BT. When the films are oxidized, a weak-but-distinguishable peak appears at 405 cm^{-1}. This feature is assigned to the υ_1 C–S mode of heterocyclic S, bound to a benzene ring [31], indicating that BT desorbs from the metal surface, but remains nearby in a hydrophobic layer between the surface and the aqueous electrolyte, as has been observed previously [19]. Platinum films exhibit this Raman peak during both high-potential segments of multi-cycle spectroelectrochemical experiments, while the peak only appears during the first oxidation cycle for Pt_3Co (data not shown) and Pt_4Ni films. On the alloys, less BT readsorbs to alloy film surfaces at lower potentials, while the remaining oxidized BT diffuses into the electrolyte solution as desorbed benzenesulfonate. In the case of pure Pt films, where all of the BT eventually readsorbs at reducing potentials, the near-surface layer of BT remains completely intact through a second positive-going sweep.

3.3. CV stripping of BT from Pt and Pt alloy films

A more complete picture of potential-dependent desorption of BT from metal electrodes is obtained when Raman spectroelectrochemical data are combined with CV stripping data [19]. The CV data also provide a more direct comparison to studies of sulfur adsorption at and desorption from Pt_3Co and Pt on Vulcan carbon [21]. Films of each of the three compositions are first cleaned in 0.1 M $HClO_4$ with 10 successive CV scans after which a baseline CV at 50 mV s^{-1} is taken. The films are then exposed to aqueous 0.01 M BT for 1 h. After BT exposure, the films are reimmersed into $HClO_4$ electrolyte and 25 CV scans are used to clean the films.

The CV data for clean films, the first CV scan after BT adsorption, and the CV stripping scan at which maximum recovery is reached of all three films show varied behavior (Fig. 9, data are summarized in Table 2). The CV data for the clean electrodes show that both Pt_3Co and Pt_4Ni films have differently-shaped CV features than the pure Pt films at potentials negative of ~400 mV, which is the potential range where the underpotential deposition and desorption of hydrogen (H_{UPD}) occurs. These differences in H_{UPD} features between the alloy films and the pure Pt films are consistent with

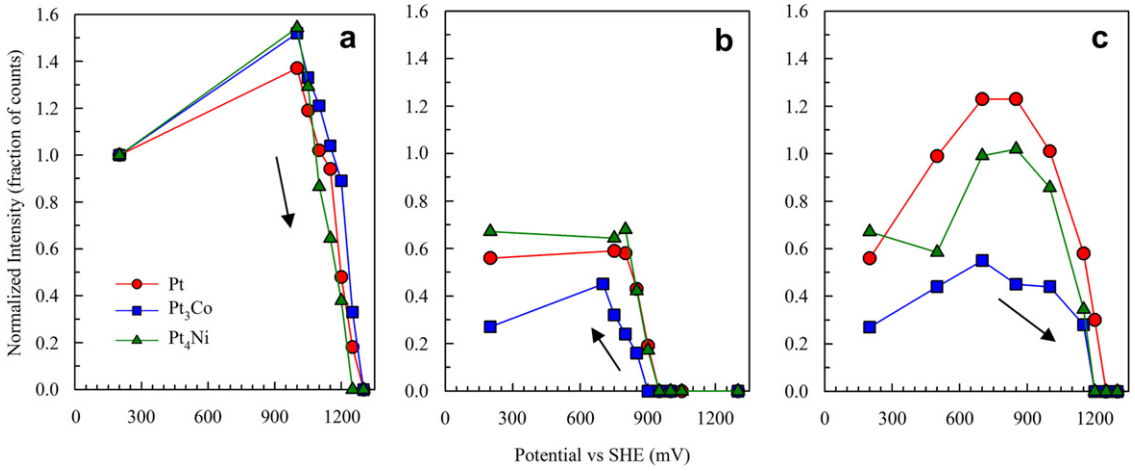

Fig. 7. Relative intensities of the 1570 cm^{-1} BT Raman peak for all of the voltages studied during positive-going and negative-going scans for Pt (●), Pt_3Co (■), and Pt_4Ni (▲) films exposed to 0.01 M BT solution for 1 h. Measurements were made in 50 mV increments in a) the desorption and b) readsorption regions of the first electrochemical cycle (1000–1300 mV and 1050–700 mV, respectively) and 150 mV increments during c) the second positive-going sweep.

those observed by Moffat et al. for the initial CV cycles of freshly deposited films [9]. The effect of BT poisoning in the BT-exposed films is obvious in the hydrogen region, where the H_{UPD} current is suppressed due to BT coverage. In agreement with predictions and observations by Pillay et al. [13], the Pt_3Co and Pt_4Ni films are initially more poisoned by exposure to S species—exhibiting ~9% and 2.5% of initial H_{UPD} activity, respectively—than Pt, which maintains ~21.5% of its H_{UPD} desorption activity. The Pt film, however, only recovers all of the initial H_{UPD} activity after 17 CV cycles, the highest number required of any of the three compositions. The Pt_3Co films recover 100% of their initial H_{UPD} activity after 14 cycles and, after an additional 3–6 scans, reach a H_{UPD} activity that is higher than before BT poisoning. This increase in apparent Pt surface area is attributed to Co leaching from the film while at oxidizing potentials, exposing more Pt surface atoms [21]. The Pt_4Ni films recover 91 ± 5% of their initial H_{UPD} activity in 10 ± 1 CV cycles, which is the fewest number of scans required to reach maximum recovery for any of the film compositions. This result is consistent with published density functional theory (DFT) calculations that propose that PtNi alloy films are less damaged by S adsorption than films containing only Pt [34]. Unlike at Pt_3Co, the H_{UPD} signal does not fully recover after electrochemically stripping BT from Pt_4Ni. This lack of recovery is in accord with the observation by Moffat et al. that Ni does not leach out of the films at substantial rates at higher potentials during the CV stripping procedure, instead forming metastable, insoluble NiO species that can persist at low potentials [9,35].

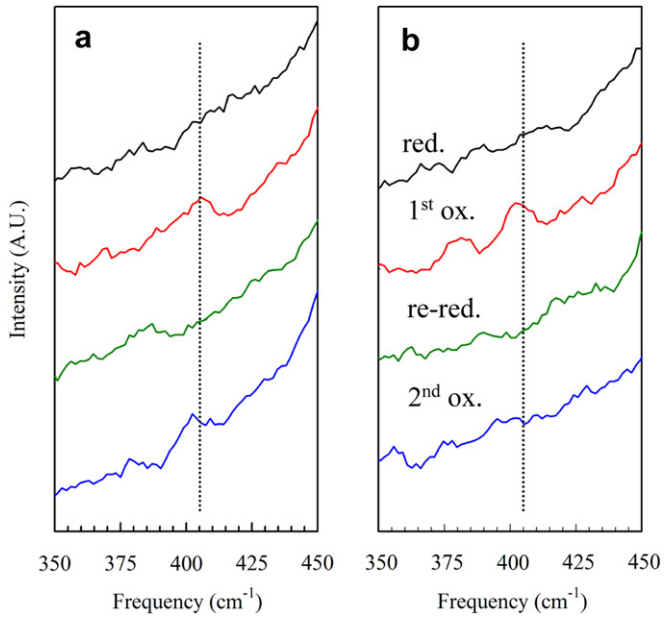

Fig. 8. The low-frequency region of *in situ* Raman spectra of a) Pt and b) Pt_4Ni films exposed to BT. The peak at 405 cm^{-1} on both films is assigned to the υ_1 C–S mode of a free benzene ring. The presence of the peak when the Pt film—but not the Pt_4Ni film—is oxidized a second time, indicates that sulfur species are more easily stripped from Pt_4Ni films and never readsorb. The data are smoothed using a 7-point box algorithm for clarity. Pt_3Co data are not shown, but are similar to the Pt_4Ni data.

The CV data also reveal that the onset potential for oxidation on a BT-poisoned Pt film is 480 mV, with the slope of the oxidation wave greatly increasing at 950 mV, while oxidation of the BT-exposed Pt_3Co film starts at 385 mV, and the Pt_4Ni film begins to oxidize at 350 mV. The more negative onset potentials for the alloy oxidation processes agree with the spectroelectrochemical data. The loss of the BT Raman signal intensity from the alloy films occurs at lower potentials than from the Pt film, as was also observed spectroscopically during the second series of positive-going potential increments (Fig. 7). The readsorption of BT to the alloy films as observed in the spectroelectrochemical measurements is also corroborated by the CV data. The peak potential for the reduction of Pt oxide on the Pt film is 925 mV, which is 35 mV higher than that on the Pt_4Ni film and 85 mV higher than for the Pt_3Co film (Fig. 9). These differences correlate very well to the ~−50 mV difference in BT readsorption to Pt_3Co films relative to that for Pt and Pt_4Ni, as shown in Fig. 7.

Moffat et al. [9] studied similar alloy films and found that they are more ORR active than Pt films. While they did not investigate the S tolerance of the films, electrodeposited thin metal films were shown to be a viable and convenient alternative to supported nanoparticles for the study of the relative activity of Pt alloys compared to pure Pt. Raman spectroelectrochemical data collectively serve as an optical counterpart to the studies of S poisoning of Pt and Pt alloy nanoparticles [13,21,34] with our CV stripping measurements serving as a bridge between the studies. The films in our study are not as easily cleaned as the supported Pt and Pt alloy nanoparticles studied by Baturina et al. [21]; their results indicate that H_2 activity is restored to alloy nanoparticles after 4–8 CV

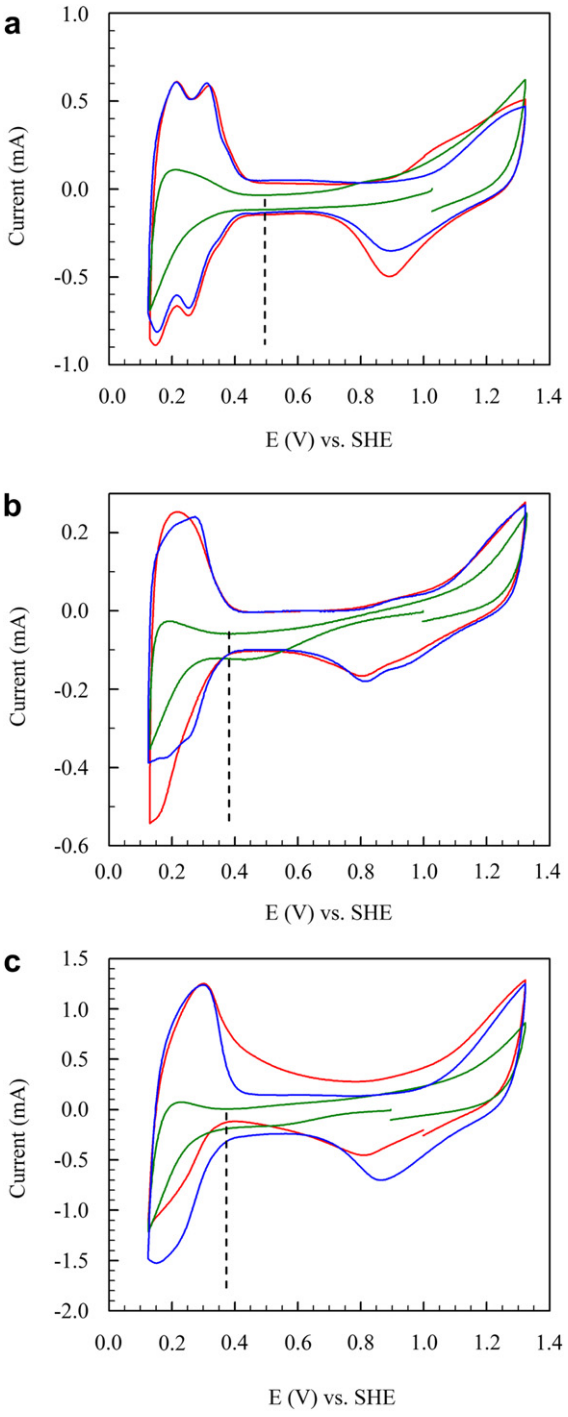

Fig. 9. Cyclic voltammograms of a) Pt, b) Pt_3Co, and c) Pt_4Ni films normalized to their electrochemical surface areas for comparison of electrochemical processes at each film. The data are shown for clean films (red trace), the first scan after BT exposure (green trace), and the scan during which the films reach their maximum recovered H_{upd} currents (blue trace). Scan rate: 50 mV s^{-1}. (For interpretation of the references to colour in this figure legend, the reader is referred to the web version of this article.)

scans, depending on the composition of the catalyst. By contrast, our films require 10–17 CV scans. Some of this difference is due to the fact that oxide formation occurs on Pt nanoparticles at more negative potentials than on bulk Pt [36], rendering the oxidative stripping of S from Pt nanoparticle surfaces more facile than from bulk Pt. Additionally, the adsorbed sulfur species studied by Baturina et al. were derived from H_2S and SO_2, which will deposit

Table 2
CV stripping analysis.

Film	1st scan activity (%)	1st scan liftoff (mV)	100% recovery scan	Max. recovery scan	Max recovered activity (%)
Pt	21.4 (0.8)[a]	480 (5)	n/a	17 (2)	98 (4)
Pt_3Co	8.8 (0.2)	379 (4)	14 (1)	18 (2)	104 (2)
Pt_4Ni	2.3 (0.6)	367 (12)	n/a	11 (1)	91 (5)

[a] Uncertainties are given in parentheses.

elemental sulfur and sulfides on the surface that when oxidized form water-soluble sulfates [21]. In contrast, adsorbed BT is oxidized to benzenesulfonic acid, which as described above, forms a hydrophobic film near the electrode when protonated. Because nonspecifically adsorbed benzenesulfonic acid readsorbs as BT when both it and the metal film are reduced [19], it is more difficult to remove electrochemically than elemental sulfur. Even taking into account these experimental differences, the same general observation that sulfur is more readily removed from Pt_3Co alloys than from pure Pt is demonstrated by the two studies.

While there is no analogous experimental study of PtNi alloy films, the DFT calculations of Pillay et al. do allow a comparison [34]. Those calculations compared the adsorption of both S and H on the (111) surfaces of Pt and Pt_3Ni, and predicted that both H and S adsorb more weakly to Pt_3Ni than to Pt. Furthermore, H and S can be co-adsorbed nearer to each other on Pt_3Ni and the Pt_3Ni surface has a lower energy barrier associated with the formation of H_2S [34]. These observations support their conclusion that the Pt_3Ni surface is easier to electrochemically clean and less affected by S poisoning than Pt alone, in accord with our findings that Pt_4Ni films are cleaned in fewer CV cycles than is pure Pt.

4. Conclusion

The combination of *in situ* Raman spectroelectrochemistry and CV stripping methods has been used to confirm that alloying Pt with Fe group metals enhances the S species tolerance of Pt. The Raman spectroelectrochemical data show that Pt_3Co is the most S-resistant of the films studied, as BT readsorbs at lower potentials during the negative-going potential increments, and less BT readsorbs to Pt_3Co than to Pt_4Ni or to Pt alone. In all films, BT desorbs through the breaking of the metal–S bond. The results of CV stripping studies confirm that the Pt, Pt_3Co, and Pt_4Ni films behave in an analogous manner to both nanoparticles and to theoretical Pt and Pt alloy surfaces in terms of adsorption and desorption of S species. The number of CV cleaning cycles required for the catalyst films to recover maximum electrocatalytic activity follows the order: $Pt_4Ni < Pt_3Co < Pt$, while the maximum extent of electrocatalytic activity recovered follows the trend: $Pt_3Co > Pt > Pt_4Ni$, both corroborating the conclusion of the spectroelectrochemical study that Pt_3Co is the most S-resistant of the electrocatalyst compositions investigated here.

Acknowledgments

Support for this work was provided by the Office of Naval Research through the U.S. Naval Research Laboratory. The authors acknowledge Nimel D. Theodore, Daniel K. Burden and Kathryn J. Wahl (NRL) for equipment use and Thomas P. Moffat (NIST), Debra R. Rolison, Jeffrey C. Owrutsky, Olga A. Baturina, Yannick Garsany, and Benjamin D. Gould (NRL) for helpful discussions.

References

[1] A. Chen, P. Holt-Hindle, Chem. Rev. 110 (2010) 3767–3804.
[2] A. Esmaeilifar, S. Rowshanzamir, M.H. Eikani, E. Ghazanfari, Energy 35 (2010) 3941–3957.
[3] M. Heitbaum, F. Glorius, I. Escher, Angew. Chem. Int. Ed. 45 (2006) 4732–4762.
[4] S. Royer, D. Duprez, ChemCatChem 3 (2011) 24–65.
[5] R. Mohtadi, W.K. Lee, S. Cowan, J.W. Van Zee, M. Murthy, Electrochem. Solid-State Lett. 6 (2003) A272–A274.
[6] V. Stamenkovic, B.S. Mun, K.J.J. Mayrhofer, P.N. Ross, N.M. Markovic, J. Rossmeisl, J. Greeley, J.K. Norskov, Angew. Chem. Int. Ed. 45 (2006) 2897–2901.
[7] S. Hidai, M. Kobayashi, H. Niwa, Y. Harada, M. Oshima, Y. Nakamori, T. Aoki, J. Power Sources 196 (2011) 8340–8345.
[8] I. Matanovic, F.H. Garzon, N.J. Henson, J. Phys. Chem. C 115 (2011) 10640–10650.
[9] T.P. Moffat, J.J. Mallett, S.-M. Hwang, J. Electrochem. Soc. 156 (2009) B238–B251.
[10] T. Komatsu, A. Tamura, J. Catal. 258 (2008) 306–314.
[11] H.L. Li, X.H. Yu, S.T. Tu, J.Y. Yan, Z.D. Wang, Appl. Catal. A 387 (2010) 215–223.
[12] S.H. Lu, C. Zhang, Y.A. Liu, Int. J. Hydrogen Energy 36 (2011) 1939–1948.
[13] D. Pillay, M.D. Johannes, Y. Garsany, K.E. Swider-Lyons, J. Phys. Chem. C 114 (2010) 7822–7830.
[14] H. Matic, A. Lundblad, G. Lindbergh, P. Jacobsson, Electrochem. Solid-State Lett. 8 (2005) A5–A7.
[15] M.B. Pomfret, J.C. Owrutsky, R.A. Walker, Anal. Chem. 79 (2007) 2367–2372.
[16] H.Y.H. Chan, S. Zou, M.J. Weaver, J. Phys. Chem. B 103 (1999) 11141–11151.
[17] X. Gao, Y. Zhang, M.J. Weaver, Langmuir 8 (1992) 668–672.
[18] R. Gomez, J. Solla-Gullon, J.M. Perez, A. Aldaz, J. Raman Spectrosc. 36 (2005) 613–622.
[19] M.B. Pomfret, J.J. Pietron, J.C. Owrutsky, Langmuir 26 (2010) 6809–6817.
[20] J.-Z. Zheng, B. Ren, D.-Y. Wu, Z.-Q. Tian, J. Electroanal. Chem. 574 (2005) 285.
[21] O.A. Baturina, B.D. Gould, Y. Garsany, K.E. Swider-Lyons, Electrochim. Acta 55 (2010) 6676–6686.
[22] D.E. Ramaker, D. Gatewood, A. Korovina, Y. Garsany, K.E. Swider-Lyons, J. Phys. Chem. C 114 (2010) 11886–11897.
[23] K.S. An, A. Kimura, K. Ono, N. Kamakura, A. Kakizaki, C.Y. Park, K. Tanaka, Surf. Sci. 401 (1998) 336–343.
[24] A.K. Shukla, M. Neergat, P. Bera, V. Jayaram, M.S. Hedge, J. Electroanal. Chem. 504 (2001) 111–119.
[25] C.D. Wagner, A.V. Naumkin, A. Kraut-Vass, J.W. Allison, C.J. Powell, J. Rumble Jr., NIST X-ray Photoelectron Spectroscopy Database, Version 3.5 (2007).
[26] D.A. Shirley, R.L. Martin, S.P. Kowalczyk, F.R. McFeely, L. Ley, Phys. Rev. B 15 (1977) 544–552.
[27] C.J. Corcoran, H. Tavassol, M.A. Rigsby, P.S. Bagus, A. Wieckowski, J. Power Sources 195 (2010) 7856–7879.
[28] K.W. Park, J.H. Choi, B.K. Kwon, S.A. Lee, Y.E. Sung, H.Y. Ha, S.A. Hong, H. Kim, A. Wieckowski, J. Phys. Chem. B 106 (2002) 1869–1877.
[29] J. Solla-Gullon, E. Gomez, E. Valles, A. Aldaz, J.M. Feliu, J. Nanopart. Res. 12 (2010) 1149–1159.
[30] K.T. Carron, L.G. Hurley, J. Phys. Chem. 95 (1991) 9979–9984.
[31] C.A. Szafranski, W. Tanner, P.E. Laibinis, R.L. Garrell, Langmuir 14 (1998) 3570–3579.
[32] S.W. Han, S.J. Lee, K. Kim, Langmuir 17 (2001) 6981–6987.
[33] Z. Jian-Zhou, R. Bin, W. De-Yin, T. Zhong-Qun, J. Electroanal. Chem. 574 (2005) 285–289.
[34] D. Pillay, M.D. Johannes, Surf. Sci. 602 (2008) 2752–2757.
[35] M.Y. Rusanova, P. Polaskova, M. Muzikar, W.R. Fawcett, Electrochim. Acta 51 (2006) 3097–3101.
[36] K.J.J. Mayrhofer, B.B. Blizanac, M. Arenz, V.R. Stamenkovic, P.N. Ross, N.M. Markovic, J. Phys. Chem. B 109 (2005) 14433–14440.